Journal of Fluorescence (2019) 29:631–643
https://doi.org/10.1007/s10895-019-02360-w

ORIGINAL ARTICLE

Environmentally Benign Carbon Nanodots Prepared from Lemon for the Sensitive and Selective Fluorescence Detection of Fe(III) and Tannic Acid

S. Stanly John Xavier[1] · T. Raj kumar[1] · M. Ranjani[1] · Dong Jin Yoo[2] · V. Archana[1] · L. Charles[1] · J. Annaraj[3] · G. Gnana kumar[1]

Received: 21 July 2018 / Accepted: 20 February 2019 / Published online: 16 April 2019

Abstract

Photoluminescent carbon nanodots (CNDs) were prepared using a biocarbon source of lemon extract. The obtained CNDs are of spherical shape and are enriched with the carboxylic acid fucntionalities. CNDs exhibited a fluorescence emission at 445 nm and unveiled blue luminescence in ultraviolet excitation. The influences of pH and ionic strength toward the stability of CNDs were investigated in detail and the obtained stability authenticates their applicability in different environmental conditions. The competitive binding of Fe^{3+} with CNDs quenches the fluorescence behavior of CNDs and was further quenched with the selective complex formation of Fe^{3+} with tannic acid (TA). The interference experiments specified that CNDs-Fe^{3+} assembly selectively detected TA and the co-existing molecules have not influenced the quenching effect of TA with CNDs-Fe^{3+}. The analytical reliability of constructed sensor was validated from the recovery obtained in the range of 91.66–107.02% in real samples. Thus the low cost and environmentally benign CNDs prepared from natural biomass provide new avenues in the fluorescence detection of biologically significant metal ions and biomolecules, facilitating their competency in on-site applications of real environmental samples.

Keywords Carbon nanodots · Competitiveness · Fluorescence quenching · Real sample analysis · Selectivity

Introduction

Carbon nanodots (CNDs) have received enormous anticipation in the recent years, paving innovative dimensions in research and practical utilities in number of applications, owing to their unique properties including easier functionalization, robust chemical inertness, low toxicity, high aqueous solubility, and excellent luminescence and optical properties [1]. The explicit interest on CNDs as fluorescent probes is enormously grown in biosensors, owing to the aforementioned advantageous features associated with its biocompatibility [2]. The unique properties of CNDs are purely governed by its quasi-spherical shape, size, abundant surface functional groups, and surface energy traps [2, 3]. It has continuously inspired the rapid advancement of novel

S. Stanly John Xavier and T. Raj kumar contributed equally to this work.

✉ Dong Jin Yoo
djyoo@jbnu.ac.kr

✉ G. Gnana kumar
kumarg2006@gmail.com

S. Stanly John Xavier
stanly.chem@gmail.com

T. Raj kumar
rajvinayagam@gmail.com

M. Ranjani
ranjichem1991@gmail.com

V. Archana
avigneshvikki93@gmail.com

L. Charles
l.charles148@gmail.com

J. Annaraj
sarokamal@gmail.com

[1] Department of Physical Chemistry, School of Chemistry, Madurai Kamaraj University, Madurai, Tamil Nadu 625021, India

[2] Department of Life Science, Department of Energy Storage/ Conversion Engineering of Graduate School, and Hydrogen and Fuel Cell Research Center, Chonbuk National University, Jeollabuk-do 54896, Republic of Korea

[3] Department of Materials Science, School of Chemistry, Madurai Kamaraj University, Madurai, Tamil Nadu 625021, India

approaches towards the preparation of CNDs with the desirable unique properties. Although CNDs were prepared from poly ethylene glycol [4], 1,2-ethanediamine [5], ethylenediaminetetraacetic acid [6], poly(ethylenimine) [7], and dopamine [8], the relevant CNDs exhibited high toxicity due to the hazardous behavior of corresponding organic sources, which additionally increased the toxicity of an entire sensor system. The significant objective of fluorescence sensors is envisioned to monitor and assess the exposure of toxic molecular species in an environment. The utilization of aforementioned toxic fluorescence probes significantly deviated the main objective of fluorescence sensors, which necessitated the development of environmentally benign CNDs from the naturally available biomass resources.

The precise and consistent recognition of biomolecules is highly significant for the perspectives including human health, sustainable development, and benign environment. Tannic acid (TA) is a naturally available polyphenolic compound, widely distributed in plants, vegetables, and fruits [9]. TA is extensively exploited as an additive, clarifying and flavouring agent in the food and medicinal products, owing to the potent astringent, diuretics, and anti-inflammtory activities [10]. As a food additive, the safety dosage of TA should be maintained in the range of 10–400 ppm in food products [11]. However, an increasing focus on commercial profitability compelled the utilization of excess quantity of TA in the manufacturing process of beer and wine for the improved color stabilization and taste enhancement. Adversely, the excess consumption of TA leads to hepatotoxic effect, liver damage, nausea, cancer, reduction in digestive enzymes activities etc., [12]. Furthermore, the toxic complex formation of TA with chromium(III) ions in leather industries pollute water bodies in the environment, which may be hazardous to the aquatic microorganisms [13]. Hence, an accurate detection of TA in food, water, beverages, and medicinal products is always been of great importance. On the basis of above, several techniques including electrochemical [14], colorimetric [15], high performance liquid chromatography [16], and chemiluminescence [17] have been adopted for TA sensing. Nevertheless, they intrinsically suffer with low efficiency, mediocre sensitivity and selectivity, requirement of sophisticated instruments, labor intensiveness, time consumption, and high cost [14–17]. Recently, fluorescence technique has been emerged as one of the most prominent method in sensing of biomolecules with the unique features of ultra-sensitive, quick response, high accuracy, less expensive, and simple operation [18]. Ahmed et al., developed the amine passivated CNDs through the thermal carbonization of 6-bromohexylboronic acid and polyethyleneglycolbis (3-amino propyl) and 1,2-diaminopropane [19]. However, the involvement of toxic chemicals and passivating reagents, tedious pre-treatment steps, and complicated purification steps hindered the on-site applications of amine passivated CNDs. Apart from the aforementioned effort, a significant impetus has not been paid toward the fluorescence detection of TA, which has not only faded the interest on fluorometric technique, but has also declined the accurate detection of TA. Hence, it is clear that the seeking of efficient fluorescence probes with low cost, high sensitivity, and considerable selectivity is still vibrant in the burgeoning field of TA sensors**.** Accordingly, we report here the development of efficient fluorescence CNDs via the simple one-pot technique by using lemon extract as a carbon source. This report is intended to analyze the influence of CNDs toward the sensitivity and selectivity in the fluorescence detection of TA and embark their on-site applications in real samples.

Experimental Section

Materials

Tannic acid (TA) (99.5%), dopamine hydrochloride (DA) (99%), uric acid (UA) (99%), sucrose (SU) (99.5%), fructose (FR) (99%), glucose (GL) (99.5%), silver nitrate ($AgNO_3$) (99.99%), aluminium nitrate ($Al(NO_3)_3$) (99.99%) and chromium(III)nitrate ($Cr(NO_3)_3$) (99.99%) were obtained from Sigma Aldrich (USA). Oxalic acid (OA) (99.5%), citric acid (CA) (99.5%), copper(II)chloride ($CuCl_2$) (99.99%), nickel(II)chloride ($NiCl_2$) (99.99%), cobalt chloride ($CoCl_2$) (99.99%), ferric(III)chloride ($FeCl_3$) (99.99%), ferrous(II)sulphate ($FeSO_4$) (99.99%) and sodium chloride (NaCl) (99.5%) were acquired from Merck and employed without any additional refinement.

Preparation of CNDs

The citrus fruit lemon obtained from local premises (Madurai, South India) was squeezed and the obtained extract was filtered via the Whatman filter paper. The hydrothermal treatment of 20 mL pulp free lemon extract at 160 °C for 3 h generates the CNDs. The resultant product was collected by removing the non-fluorescent large particles through filtration with 0.22 μm filter membrane and the prepared CNDs were stored at 4 °C for further analysis.

Characterizations

The prepared CNDs were tested with transmission electron microscopy (TEM, JEOL-JEM-2010), X-ray diffractometer (Rigaku-D-Max-2500), Fourier transform infrared (FT-IR) spectroscopy (Jasco-300E), Raman spectrometer (JY-HR800), and UV-*vis* spectrometer (Agilent-8453).

Sensor Studies

In a typical procedure, an appropriate amount of Fe^{3+} ions with different concentrations was gradually added to the

prepared CNDs (1 mg.mL^{-1}). The fluorescence quenching was observed with the addition of Fe^{3+} ions and was saturated with 465 μM Fe^{3+} ions. Hence, 465 μM of Fe^{3+} was used as the optimal concentration for the further sensing of TA molecules. To evaluate the sensitivity of CNDs-Fe^{3+} assembly towards TA, different concentrations of TA in the range of 1–265 μM was gradually added to the CNDs-Fe^{3+} assembly. The corresponding fluorescence spectra were consecutively recorded using Agilent Cary Eclipse fluorescence spectrophotometer. The detection limit was calculated with a formula of 3σ/K, where σ is the standard deviation for ten consecutive fluorescent measurements of blank solution and K is the slope of a calibration curve [20].

Lifetime Measurement Studies

The lifetime measurements were achieved with Horiba fluorolog3TCSPC fluorescence spectrophotometer and the lifetime (τ) was calculated with an equation of:

$$\tau = T_1B_1 + T_2B_2 + T_3B_3\ldots./100 \quad (1)$$

where T and B specify, respectively, time and relative amplitude.

The absolute quantum yields of studied CNDs were deliberated using Edinburgh FLS-980 spectrometer with a 450 W xenon lamp. With an equation of $\eta = [(E_B - E_A)/(S_A - S_B)] \times 100$, the absolute fluorescence quantum yield was estimated. Where absolute fluorescence quantum yield (η), indices to the reference sample (deionized water) and CNDs ("A" and "B"), and the integral of scans (S_A, S_B E_A, and E_B) are specified.

Results and Discussion

Synthesis and Characterizations of CNDs

The fluorescent CNDs were prepared by using one-pot hydrothermal technique with the aid of a lemon extract as a renewable, inexpensive, and environmentally benign single carbon source. The formation mechanism of CNDs involves the hydrothermal carbonization of compounds exist in the lemon fruit extract. The components of lemon extract such as citric acid and ascorbic acid are converted into CNDs through the dehydration, polymerization, condensation, and carbonization processes [21]. The hydrothermal carbonization of lemon extract yields a pale yellow color solution (Inset: Fig. 1a(i)) and exhibits the bright blue emission under UV irradiation. CNDs exhibit a UV-*vis* band (282 nm) (Fig. 1a(i)) because of the C=C bond (π-π* transition) [21]. The addition of Fe^{3+} in CNDs decrease the intensity of a characteristic absorption band of CNDs (Fig. 1a(ii)) and provides the intense yellow color solution (Inset: Fig. 1a(ii)). CNDs-Fe^{3+}-TA exhibits a new broad absorption band at 585 nm (Fig. 1a(iii)), owing to the complex formation between TA and CNDs-Fe^{3+} assembly [22] and offers the greenish black color (Inset: Fig. 1a(iii)). The strong blue emission observed for CNDs is partially quenched with Fe^{3+} ions and is completely quenched with TA with the aid of CNDs-Fe^{3+} assembly under UV radiation (365 nm) (Fig. 1a(iii)).

From the dependence behavior of excitation wavelength (Fig. 1b), it is observed that the emission spectra of CNDs are responsive with the excitation wavelength and are varied from 403 to 508 nm with an increase in the excitation wavelength from 280 to 440 nm. Upon the increase of excitation wavelength (λ_{ex}) from 280 to 350 nm, the intensity of emission peaks is enhanced and red-shifted. When λ_{ex} ranges between

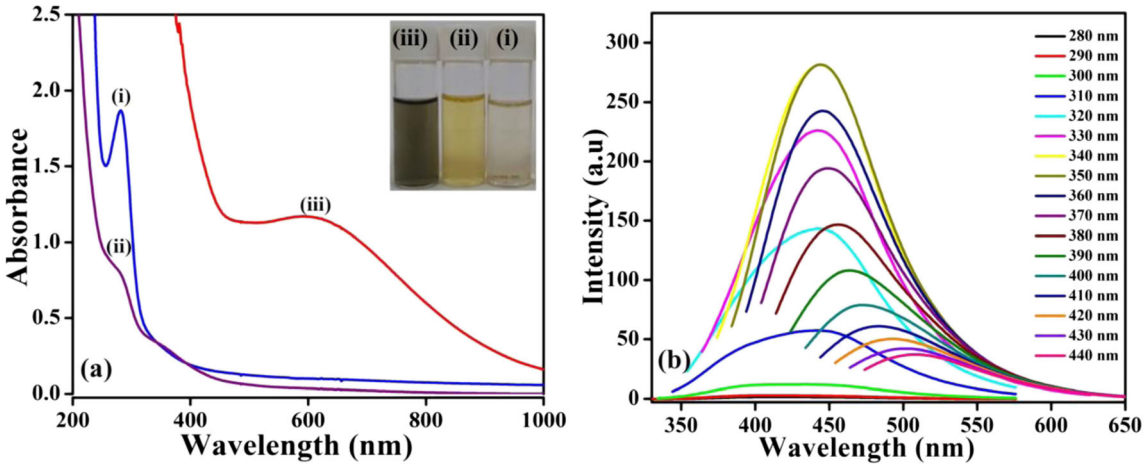

Fig. 1 **a** UV-*vis* spectra of (i) CNDs, (ii) CNDs-Fe^{3+} and (iii) CNDs-Fe^{3+}-TA (Inset: corresponding optical photographs under daylight lamp), and **(b)** emission spectra of CNDs at various λex

350 to 440 nm, the relevant peak positions are altered to a longer wavelength region associated of the lowered intensities, depicting multi-emissive characteristics of CNDs. It is due to the confined quantum effect and widened emissive entangles on CNDs [23]. The fluorescence characteristics of CNDs are originated via radiative recombination of excitons, quantum effect, different emissive traps or states, and oxygen labile functional groups [24]. The photo-luminescence quantum yield (absolute) of CNDs, CNDs-Fe^{3+}, and CNDs-Fe^{3+}-TA is found, respectively, to be 17, 1.4, and 0.05%. The prepared CNDs exhibit a high quantum yield, detailing an excellent florescence quality of CNDs because of self-passivated oxygen functionalities on CNDs [25, 26]. It is also evidenced via bright blue emission obtained with UV radiation (365 nm) (Fig. 2 and Inset: Fig. 2(i)). The addition of TA with CNDs slightly quenches the fluorescence behavior of CNDs (Fig. 2 and Inset: Fig. 2(ii)). The visualized quantitative quenching of blue fluorescence under UV radiation upon the introduction of Fe^{3+} ions into CNDs is well supported from the decrement of quantum yield (Fig. 2 and Inset: Fig. 2(iii)), ascribing to the binding of Fe^{3+} ions with CNDs. Upon the addition of TA into CNDs-Fe^{3+}, the rapid decrement in quantum yield was observed, which is eventually validated from the complete quenching of blue fluorescence (Fig. 2 and Inset: Fig. 2(iv)), because of the complex configuration of TA with CNDs-Fe^{3+} assembly.

The prepared CNDs are spherical with a mean diameter of 3 nm (Fig. 3a, b). The ordered lattice fringes (d-spacing = 0.22 nm) are observed (Inset: Fig. 3c(i)) for the prepared CNDs (Fig. 3c) ascribed to (102) facet of graphitic (sp^2) carbon. The obtained SAED pattern (Inset: Fig. 3c(ii)) with broad diffraction ring patterns confirms the polycrystalline structure of CNDs.

The prepared CNDs exhibit a distinctive carbonaceous (002) reflection plane [24] and the CND's lattice spacing (0.39 nm) is superior compared to the graphite interlayer spacing (0.34 nm) due to the existence of oxygen labile functional groups on CNDs [27]. Decreasing the intensity of a characteristic carbonaceous diffraction peak along with an increment in broadness are sequentially observed for CNDs-Fe^{3+} (Fig. 3d(ii)) and CNDs-Fe^{3+}-TA (Fig. 3d(iii)).

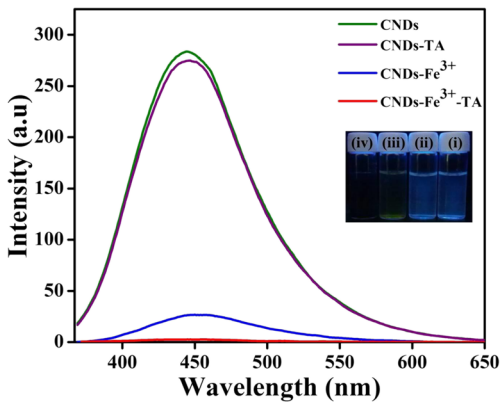

Fig. 2 Fluorescence emission of studied nanostructures (Inset: Optical photographs of (i) CNDs, (ii) CNDs-TA (iii) CNDs-Fe^{3+} and (iv) CNDs-Fe^{3+}-TA under 365 nm UV excitation)

CNDs exhibit the characteristic carbonaceous Raman bands at 1354 and 1566 cm^{-1} (Fig. 3e(i)), which are ascribed, respectively, to the D and G bands of graphite. The D band connects the carbon atom's vibration with tangling bonds, whereas G band connected with E2g mode of the vibration of sp2-hybridized carbon atoms [6]. The relative intensity (I_D/I_G) of CNDs-Fe^{3+} is estimated as 0.84, which is higher than that of CNDs (0.75), specifying that the interaction of CNDs with Fe^{3+} ions generates the disordered carbon structure [17] (Fig. 3e(ii)). A further increment in I_D/I_G ratio of 0.98 is observed for CNDs-Fe^{3+}-TA (Fig. 3e(iii)), representing the growth of coarse like carbon particles.

CNDs exhibit the characteristic carbonyl stretching vibration at 1720 cm^{-1} (Fig. 3f(i)) and the 1634 and 1397 cm−1 bands represent, respectively, asymmetric and symmetric stretching vibrations of COO^-. The 1072 and 1224 cm−1 bands, represent, respectively, C-O/C-O-C and C-OH stretching vibrations [21]. The asymmetric and symmetric stretching vibrations of COO^- are sharpened and the intensities are significantly increased for CNDs-Fe^{3+} assembly (Fig. 3f(ii)). The intensity of carbonyl stretching at 1720 cm^{-1} is decreased and the C-O-C/C-O and C-OH vibrations are altered, denoting the interaction Fe^{3+} with COOH groups of CNDs [24]. The Fe-O bond is found at 589 cm^{-1}, which ensures the interaction of Fe^{3+} with COO^-/OH functionalities on the surface of CNDs [27]. The intensities of characteristic carbonyl, asymmetric and symmetric COO^- and C-O/C-O-C and C-OH stretching vibrations are further reduced with the increased broadness for CNDs-Fe^{3+}-TA (Fig. 3f(iii)), specifying the effective interaction between the hydroxyl groups of TA and CNDs-Fe^{3+} assembly [28].

The NaCl concentration of 0 to 500 mM is used to analyze the stability of CNDs (Fig. 4a). The observed fluorescence spectra elucidate the nearly constant fluorescence intensity against NaCl concentration. (Fig. 4a and Inset: Fig. 4a), specifying the robust stability of CNDs, which enables its practical sensing applications under harsh environmental conditions.

For the analysis of the impact of pH on the stability of CNDs and obtain the optimal conditions for further analytical applications, the fluorescence intensity of prepared CNDs was analyzed for a pH of 2.0−12.0 (Fig. 4b). The fluorescence intensities of prepared CNDs remain almost constant for the pH of 2−8. Upon the further increment in the pH levels, the fluorescence intensity of CNDs is slightly lowered (Fig. 4b and Inset: Fig. 4b), owing to the destruction of functional groups existing on CNDs [29], which enunciates the robust stability of prepared CNDs.

Fluorescence Detection of Fe^{3+} Ions and TA

The prepared CNDs were exploited as fluorescence probes for the detection of TA under neutral conditions and the

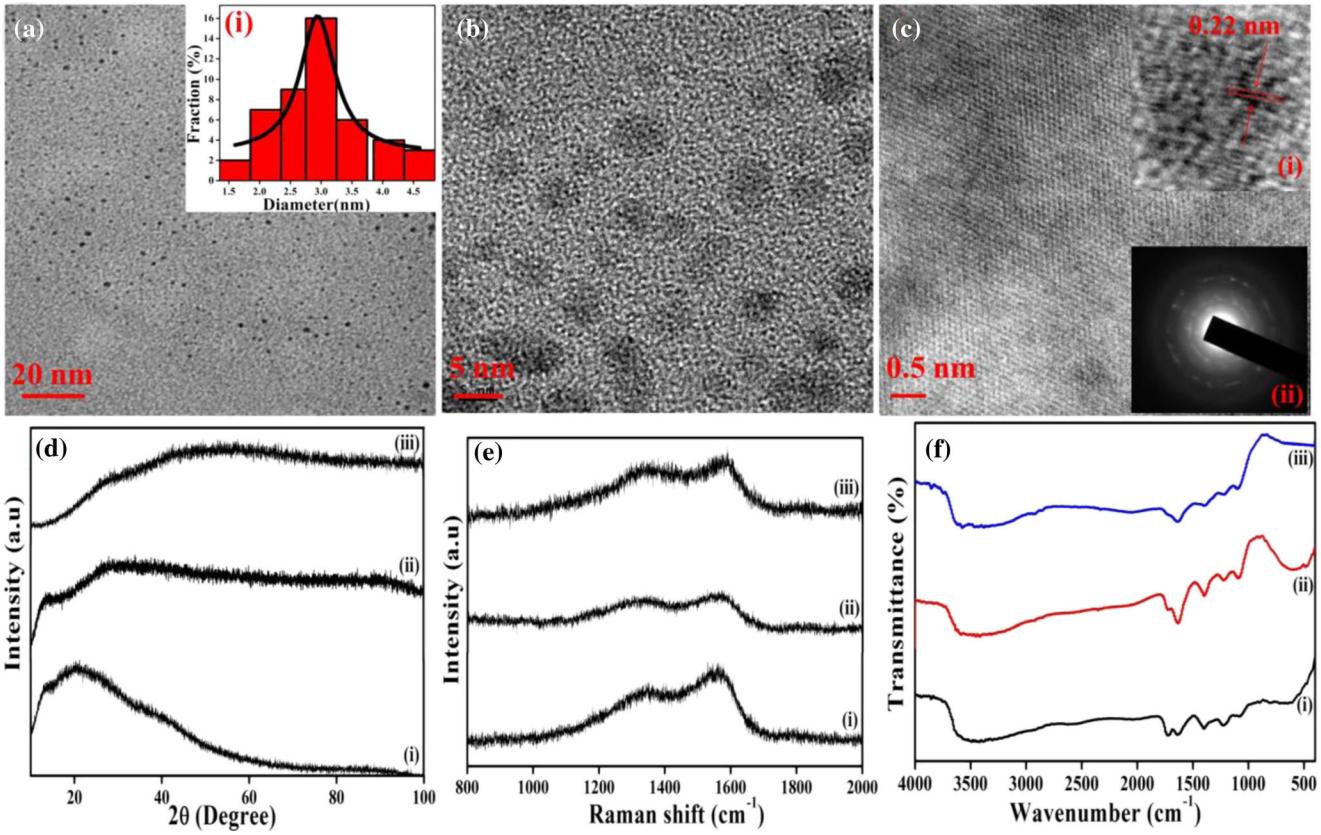

Fig. 3 **(a and b)** TEM images (Inset a: particle size histogram) and **(c)** FFT pattern of CNDs (Inset c: (i) projected FFT pattern and (ii) SAED pattern) and **(d)** XRD patterns, **(e)** Raman spectra, and **(f)** FT-IR spectra of (i) CNDs, (ii) CNDs Fe^{3+} and (iii) CNDs-Fe^{3+}-TA

fluorescence response of 265 μM TA injected CNDs was evaluated (Fig. 2). Owing to the weak hydrogen bonding between the surface carboxylic acid groups of CNDs and hydroxyl groups of TA, the minimal fluorescence quenching of CNDs is achieved without any variation in the fluorescence color (Inset: Fig. 2(ii)). The obtained fluorescence quenching for CNDs still remain as a formidable hurdle to the alluring perspective of real time sensor applications. Henceforth, an intermediate complex of CNDs is desirable to enable the strong interaction between CNDs and TA. Hence, Fe^{3+} ions are chosen for the complex formation with CNDs on the basis of its constructive characteristics including the environmentally benign character, inexpensive, and easier availability in living systems.

The fluorescence responses of prepared CNDs on Fe3+ ions concentration of 0 - 465 μM were investigated (Fig. 5a). Upon the injection of Fe^{3+} ions into CNDs, the fluorescence intensity of CNDs is strongly quenched as evidenced from the PL spectra. The aforementioned observation clearly illustrates that Fe^{3+} ions efficiently quenches the fluorescence properties of CNDs, which is presumably occurred via coordination between Fe3+ and -oxygen labile functionalities of CNDs. The involved CND's fluorescence quenching mechanism with Fe^{3+} is schematically illustrated in Fig. 6. The further increment in Fe^{3+} ions concentration does not provide any alteration of fluorescence quality of CNDs, channeling the use of 465 μM Fe^{3+} ions for farther analysis. The considerable linear behavior for 3.3 to 125 μM concentration (Inset: Fig. 5a) and detection limit of 0.44 μM are witnessed for Fe^{3+}, outfitting the previous Fe^{3+} sensing reports. (Table 1) [30–42].

Fe^{3+} is one of the significant essential transition metal ion involved in metabolic process and widely distributed in various living organisms along with Cu^{2+}, Co^{2+}, Mn^{2+}, Ni^{2+}, and Fe^{2+}, necessitating the evaluation of specific detection of constructed fluorescence probe toward Fe^{3+} ions against the common interfering metal ions [43]. Hence, the selectivity studies of prepared CNDs were achieved against the interferences including Cu^{2+}, Ag^{+}, Al^{3+}, Pb^{2+}, Co^{2+}, Cr^{3+}, Hg^{2+}, Mn^{2+}, Ni^{2+}, and Fe^{2+} at a concentration of 465 μM. From the obtained fluorescence spectra (Fig. 5b), it is clear that the substantial fluorescence quenching is observed only with Fe^{3+} ions and the other metal ions exhibit only negligible effect (Fig. 5b, c) because of the inferior interaction of CNDs with metal ions. The effective interaction of Fe^{3+} and oxygen labile functionalities of CNDs lead to splitting of d orbital of Fe^{3+} [18, 43]. It is proceeded with the partial transference of electrons in the excited state of CNDs to the d-orbital of Fe^{3+} and

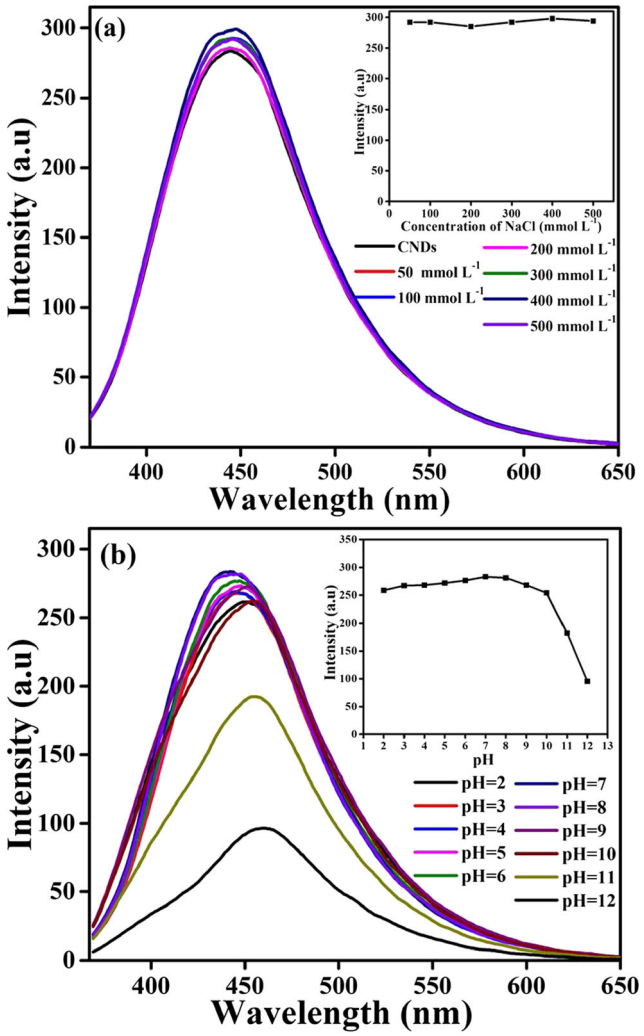

Fig. 4 The influence of **(a)** NaCl concentration (Inset: relevant linear calibration curve) and **(b)** pH levels on fluorescence characteristics of CNDs (Inset: relevant linear calibration curve)

is responsible for the high selectivity of CNDs toward Fe^{3+} ions than those of other metal ions [44]. Initially, Fe^{3+} is adsorbed on the surface of CNDs with the coordination of hydroxyl groups on the surface of CNDs, which is further followed by the transference of electrons in the excited state of CNDs to the Fe^{3+} ions. Under the UV irradiation of 365 nm, the photo induced electrons of CNDs are effectively transferred to the paramagnetic Fe^{3+} with a higher number of unfilled d-shell valence electrons, leading to the conversion of +3 state into +2 [45]. Thus the higher number of valence electrons of Fe^{3+} ions compared to the other studied cations is responsible for the non-radiative electron / hole recombination based fluorescence quenching of CNDs [45, 46]. In general, the metal ions with high positive redox potential are referred as the strong oxidants. In this context, Fe^{3+} demonstrates high positive redox potential (0.771 V) than those of other interfering metal ions including Cu^{2+} (0.340 V), Fe^{2+} (−0.44 V), Pb^{2+} (−0.126 V), Co^{2+} (−0.28 V), Cr^{3+} (−0.41 V), Mn^{2+} (−1.17 V), and Ni^{2+} (−0.257 V), which maximizes the electron transfer and responsible for the selective electron transfer based quenching with CNDs [47]**.** Although, Hg^{2+} demonstrates the high positive redox potential (0.80 V) than that of Fe^{3+}, the completely filled d orbitals of Hg^{2+} restrain its electron transfer ability with CNDs. Furthermore, the redox potential of Fe^{3+} is located between the conduction band (CB) and valence band (VB) of CNDs, stimulating the effective electron transfer from CB to Fe^{3+} [48]**,** which collectively leads to the high selectivity of CNDs toward Fe^{3+} .

The competitive test of prepared CNDs toward Fe^{3+} ions was investigated amidst of co-existing substances such as Cu^{2+}, Ag^{+}, Al^{3+}, Pb^{2+}, Co^{2+}, Cr^{3+}, Hg^{2+}, Mn^{2+}, Ni^{2+}, and Fe^{2+} (Fig. 5d). The co-existing substances do not impact the sensing performances of CNDs as supported with 89% quenching effect of Fe^{3+} ions, coinciding with the fluorscence behavior of CNDs in the absence of co-existing metal ions.

The developed CND-Fe^{3+} assemblies were manifested as the alluring fluorescent probes for TA sensing (Fig. 7a). The fluorescence behavior of CNDs-Fe^{3+} assembly displays a significant reduction in intensity at a wavelength of 445 nm with the injection of TA and exhibits a gradual reduction with the increased concentration of TA. The fluorescence intensity of CNDs is completely quenched at 265 μM TA. The electron rich TA is quickly adsorbed on the surface of CNDs-Fe^{3+} assembly and the catecholate/galloyl groups of several TA molecules facilitate an electron transfer from hydroxyl groups to CNDs-Fe^{3+} assembly [49], resulting the stable coordination complex as substantiated from the visible color change from yellowish to greenish black color (Inset: Fig. 2). The active Fe^{3+} ions on CNDs exhibits an inherent paramagnetic character with the half-filled electronic structure, leading to a strong electron accepting tendency toward TA and promotes the stronger coordination between TA and CNDs-Fe^{3+} assembly, which supports the complete quenching of fluorescence behavior of CNDs-Fe^{3+} assembly. The engaged fluorescence quenching mechanism of CNDs-Fe^{3+} assembly with TA is schematically illustrated in Fig. 6. A linear relation for the concentration of TA from 1 to 47.5 μM is observed. (Inset: Fig. 7a) and the detection limit of developed system is found as 0.31 μM, which are comparable and even better than those of previous reports (Table 2) [14, 15, 19, 50–53], authenticating their applicability in relevant sensor fields.

The efficacy of fabricated sensor probes is solely dependent upon the ability in achieving the specific detection of an analyte without any interferencing effect in real samples. Certain biomolecules such as CA, DA, GL, AA, Na^{+}, Ca^{2+}, and Mg^{2+} ions are the common interfering and co-existing species in physiological and water samples. Hence, the selectivity of prepared CNDs were analyzed against the interferences including CA, OA, DA, UA, SU, FR, GL, AA, Na^{+}, Ca^{2+}, and Mg^{2+} at a concentration of 265 μM. CNDs-Fe^{3+}

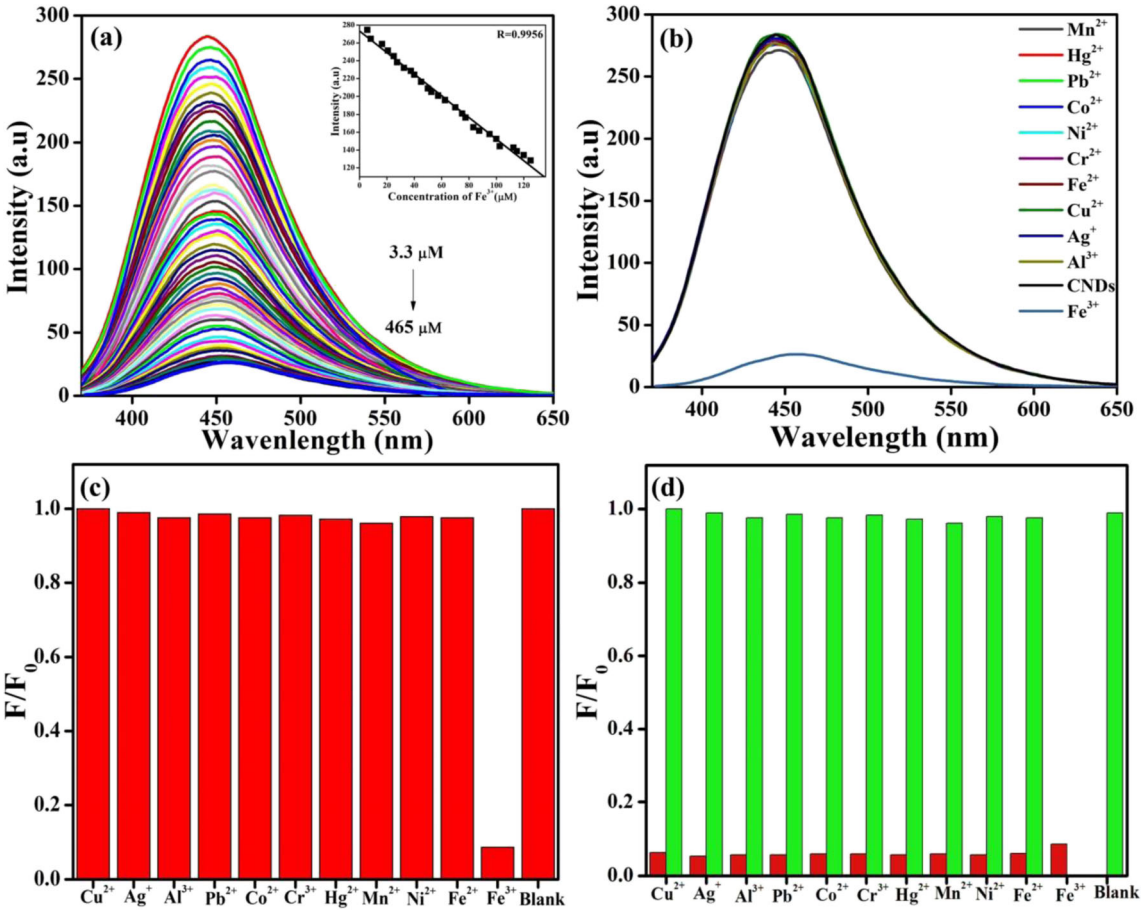

Fig. 5 **a** Fluorescence emission of CNDs with respective of distinct Fe^{3+} concentrations (Inset a: relevant linear calibration curve), (**b**) fluorescence emission spectra of CNDs in disparate interference metal ions and Fe^{3+} ions and **(c)** relevant intensity profile, and **(d)** competitive effects of 465 μM disparate interference metal ions on Fe^{3+} sensing

demonstrated nullified quenching effect with other species (Fig. 7b, c). Owing to the strong electron accepting ability, CNDs-Fe^{3+} assembly easily acquires electrons donated from the electron rich hydroxyl groups of TA. Furthermore, the rapid and stable bi-dentate chelation effect of TA with CNDs-Fe^{3+} assembly enunciates the selectivity of CNDs-Fe^{3+} assembly toward TA [54].

The competitive analysis of prepared CNDs-Fe^{3+} assembly was carried out with the co-existing molecules such as CA, OA, DA, UA, SU, FR, GL, AA, Na^{+},Ca^{2+}, and Mg^{2+} at a concentration of 265 μM and the influence of relevant co-existing biomolecules present in real samples was investigated (Fig. 7d). From the obtained results it is clear of no disturbances from the other molecules for the quenching effect of CNDs-Fe^{3+} assembly toward TA as evidenced from 90% quenching effect of TA. It is comparable with the quenching (91.5%) observed under the absence of co-existing biomolecules.

The behavior of CNDs and CNDs-Fe^{3+} toward Fe^{3+} and TA, respectively, were scrutinized with respective of time with a regular time interval of 1 min (Fig. 8). The fluorescence intensity of CNDs and CNDs-Fe^{3+} assembly was immediately quenched after the addition of Fe^{3+} (Fig. 8a, b) and TA (Fig. 8c, d), respectively, and both of the reactions were completed within a minute. After this saturation time, the characteristic spectral changes were not observed. The observed rapid response time suggests that prepared CNDs could be effectively used as an efficient fluorescent probe for the practical sensing of Fe^{3+} ions and TA.

To further investigate the reliability and potential practical applicability of proposed sensor toward the sensing of Fe^{3+} ions and TA, the developed sensor probe was tested in real environmental water sample. The water sample was collected from Vaigai-river (Madurai, India) for the recovery test with the different concentrations of Fe^{3+} and TA, respectively, in CNDs and CNDs-Fe^{3+}, to adequate the precision of developed probe (Fig. 9a, b). The fluorescence intensity is decreased with the increasing concentration of Fe^{3+} ions (Fig. 9a) and TA (Fig. 9b) and the recovery of 89.24–107.25% with the relative standard deviation (RSD) of 1.02–2.14 (n=4) for Fe^{3+} ions and 91.66–107.02% RSD of 1.01–2.95 (n=4) for TA. Thus the obtained results substantiate the onsite and real time

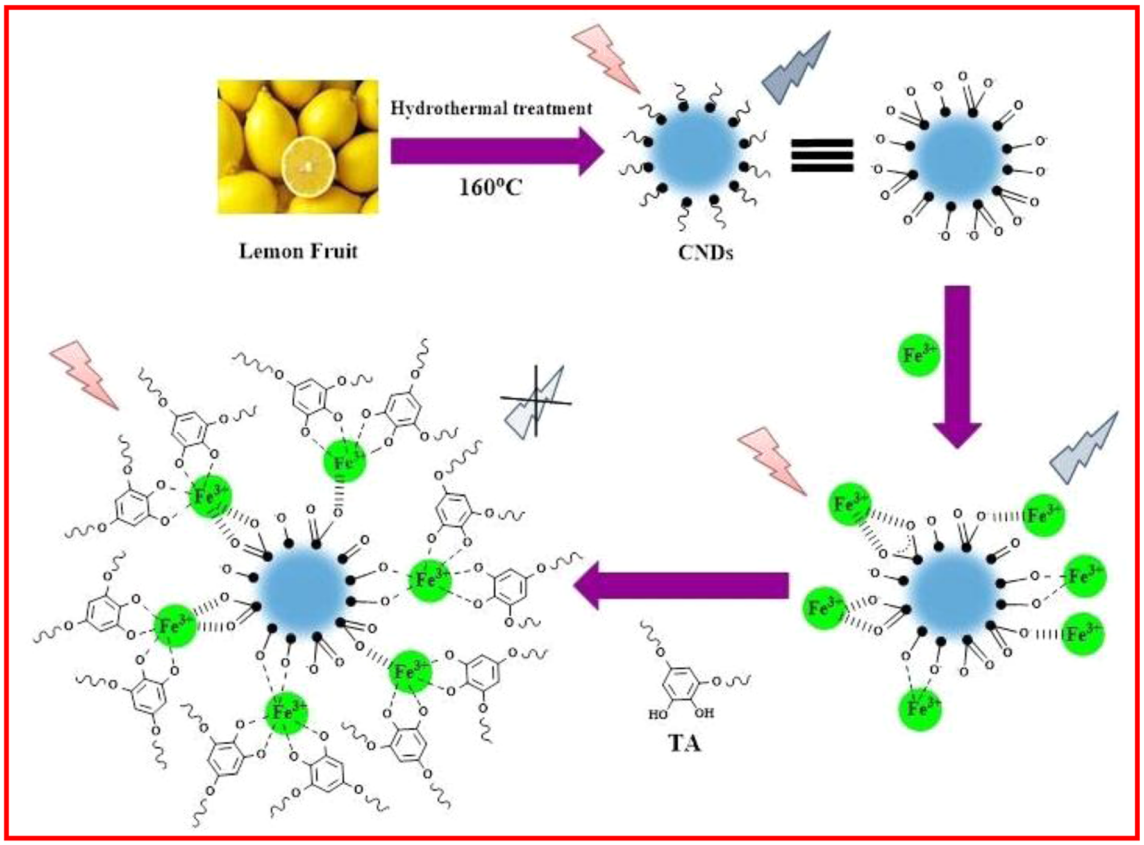

Fig. 6 Mechanism involved in the fluorescence detection of TA at CNDs

application of prepared CNDs toward the detection of Fe^{3+} ions and TA in environmental water samples.

The time correlated single photon counting (TCSPC) analysis was performed to elucidate the fluorescence quenching mechanism in amidst and absence of Fe^{3+} ions and TA (Fig. 9c). The fluorescence lifetime of prepared CNDs is 6.6 ns and the fluorescence decay time of CNDs-Fe^{3+} assembly is decreased to 6.2 ns after the coordination with Fe^{3+} ions. The decay curves of CNDs and CNDs-Fe^{3+} assembly are indistinguishable from each other, specifying that the negligible

Table 1 Comparison of the Fe^{3+} sensing performances of fluorophores

Probe	Linear range (μM)	Detection limit (μM)	Ref.
GQDs[a]	10–80	7.22	[30]
PNDs[b]	0.1-10	–	[31]
Au NCs[c]	5–1280	3.50	[32]
MIL-53 (Al) –MOF[d]	3–200	0.90	[33]
N[e]-GQDs[a]	1-70	0.08	[34]
CDs[f]	12.5–100	9.97	[35]
CDs[f]	0–6	0.40	[36]
CDs[f]	1–100	–	[37]
CNPs[g]	0–20	0.32	[38]
N[e]-CQDs[a]	0–50	4.67	[39]
CDs[f]	0–0.03	0.01	[40]
GSH[h]@AgNCs[b]	0.5-20	0.12	[41]
CNDs[i]	0-5	–	[42]
CNDs[i]	3-125	0.44	This work

[a] graphene quantum dots; [b] polymernanodots; [c] nanoclusters; [d] metal-organic frameworks; [e] nitrogen; [f] carbon dots; [g] Carbon nanoparticles; [h] glutathione; [i] carbonnanodots

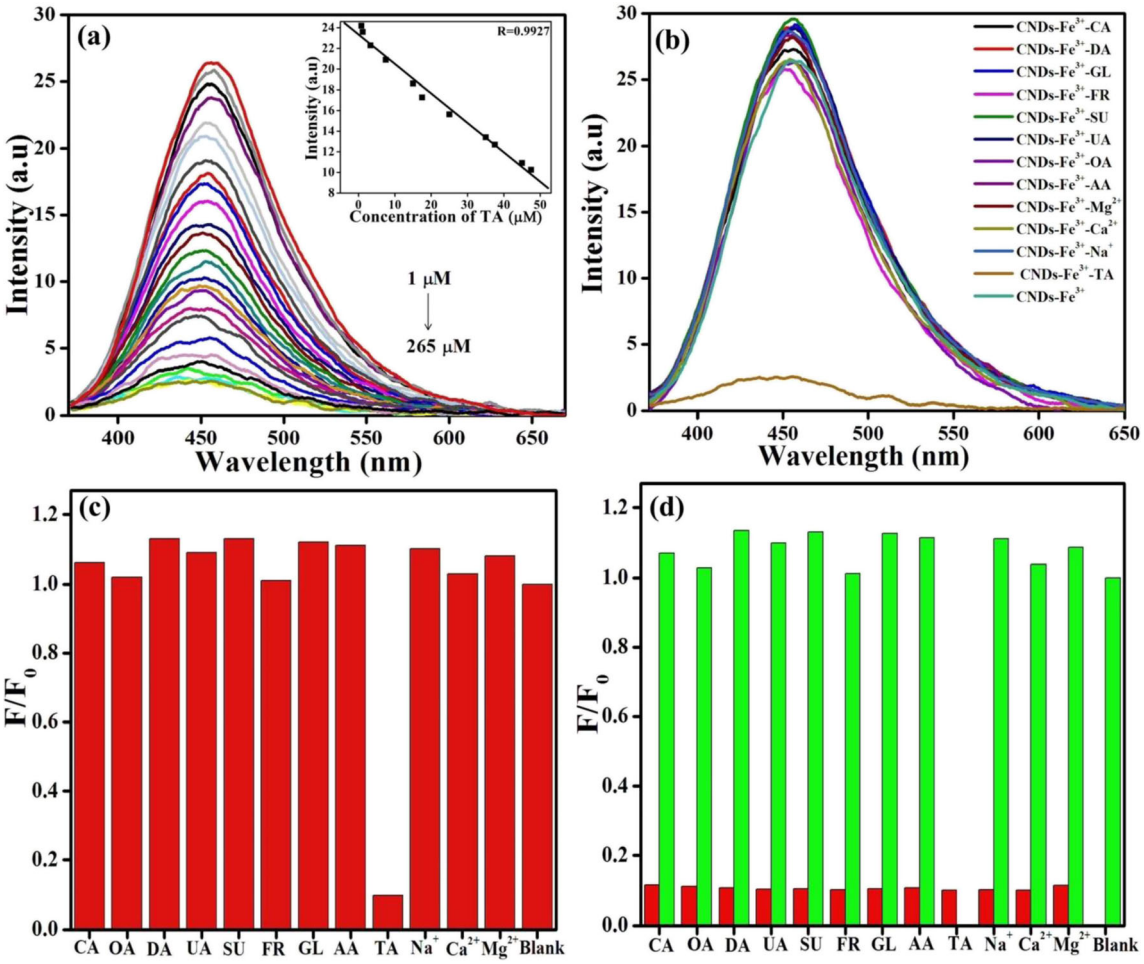

Fig. 7 **a** Fluorescence emission spectra of CNDs-Fe^{3+}assembly with respective of distinct TA concentrations (Inset a: relevant linear calibration curve), **(b)** fluorescence emission of CNDs-Fe^{3+} assembly in the distinct of 265 μM concentration of various interference biomolecules and metal ions and TA and **(c)** relevant intensity profile, and **(d)** competitive effect of 265 μM disparate interference biomolecules and metal ions on TA sensing

change in fluorescence lifetime is witnessed with the addition of Fe^{3+} ions. The less significant reduction in the lifetime and decay curves of CNDs and CNDs-Fe^{3+} assembly imply that the quenching mechanism is primarily ascribed to static, because the formation of a stable non-fluorescent coordination complex between Fe^{3+} ions and surface -COOH and -OH groups of CNDs. The fluorescence lifetime of CNDs-Fe^{3+}-TA is significantly reduced to 5.4 ns, signifying that the dynamic quenching mechanism is involved in the detection performances. It is achieved through the electron transfer and effective chelation between the hydroxyl groups of TA and CNDs-Fe^{3+} assembly.

Table 2 Comparison of the TA sensing performances of fluorophores

Probe	Linearrange (μM)	Detection limit (μM)	Ref.
3-aminophthalate	3–180	0.58	[50]
PPCPE[a]	0.01-1	0.01	[51]
Ch[b]–Ag NPs[c]	1–100	1	[15]
CNDs[d]	0.05-0.6	0.01	[19]
PrTu[e]	2–42	0.6	[14]
NCD[f]	0.07-7.0	0.026	[52]
GQDs[g]	0.1–1	0.026	[53]
CNDs[d]-Fe^{3+}	1-47.5	0.31	This Work

[a] porous pseudo-carbon paste electrode; [b] chitosan; [c] nanoparticles; [d] carbonnanodots; [e] 1-benzoyl-3-(pyrrolidine) thiourea; [f] nitrogen-doped carbon quantum dots; [g] graphene quantum dots

Ahmed et al., synthesized CNDs via a thermal carbonization of 6-bromohexylboronic acid and polyethyleneglycol bis (3-aminopropyl (PEGA) at 180 °C, followed by its purification through the dialysis process for 3 days [19]. The tedious synthetic procedures adopted for the preparation of GQDs associated with the organic derivative stimulated toxic surface to the fluorescence probe, which limited their practical applications in biological samples. The linear range of TA detection for the prepared CNDs was found to be 0.05–0.6 μM, which is inferior to the linear range of reported environmentally benign CNDs

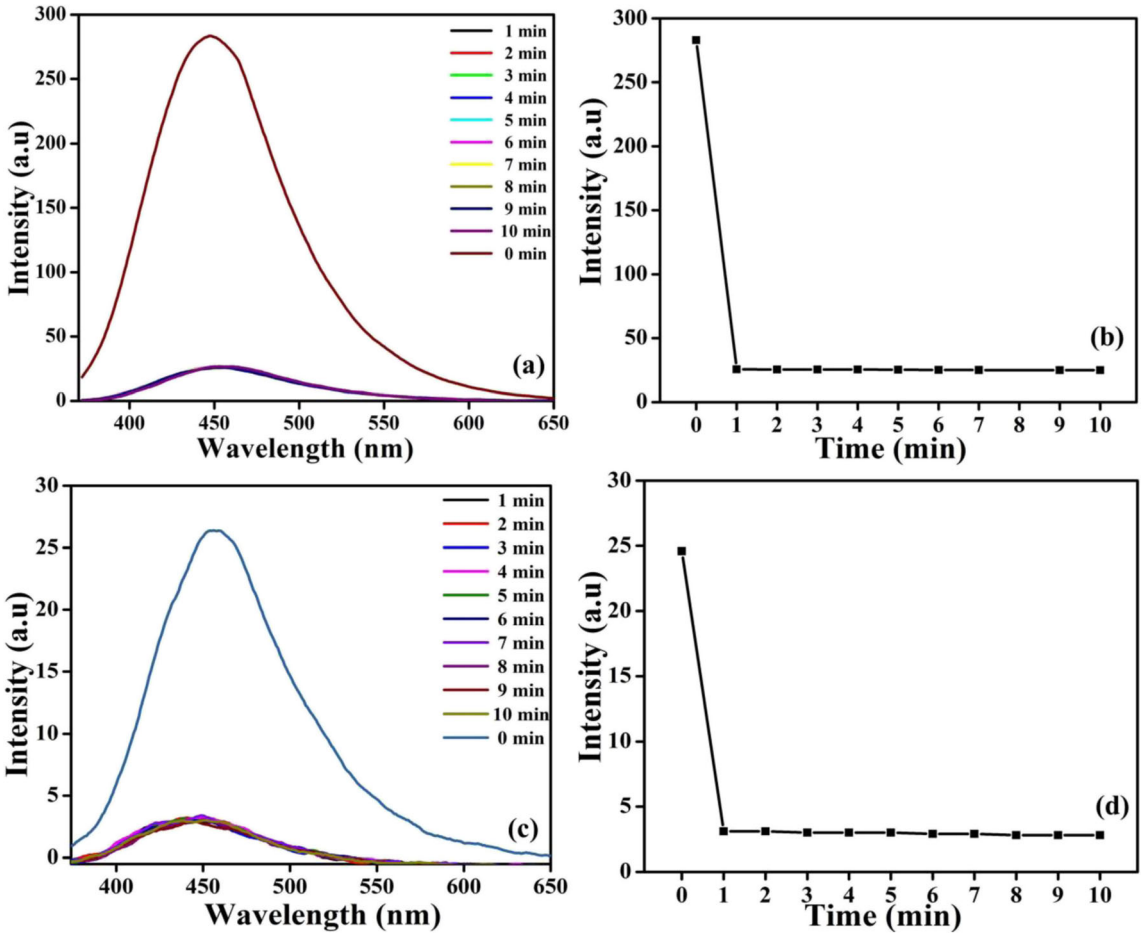

Fig. 8 **a** Fluorescence emission of CNDs with 465 μM Fe^{3+} ions with respective of time and **(b)** variation of fluorescence intensities of CNDs with 465 μM Fe^{3+} ions with respective of time, **(c)** Fluorescence emission spectra of CNDs-Fe^{3+} assembly with 265 μM TA with respective of time and **(d)** variation of fluorescence intensities of CNDs-Fe^{3+} assembly with 265 μM TA with respective of time

(1–47.5 μM) (Table 2). The aforementioned report has not detailed the competitive and lifetime measurement studies, which effectively hindered the fundamental understanding on the influences of co-existing substances toward TA sensing [19]. GQDs prepared from citric acid demonstrated an inferior linear range (0.1–1.0 μM) toward TA detection (Table 2) and the lack of competitive studies, stability under various ionic strengths, time correlated studies, and reliability test hinder their prospective on-site applications [53]. The NCNDs prepared from ascorbic acid via ultrasonic approach was used as a fluoroprobe for the detection of TA [52]. However, the inefficient selectivity accomplished between TA and TU, narrow linear range (0.07–7.0 μM) (Table 2), and the compelled utilization of $KMnO_4$ for the generation of isothiocarboamido radicals to enhancing the fluorescence signals debase the analytical performances. The quenching mechanism involved in the above reports has also not been addressed that collectively limited the realization of aforementioned reports in reliable practical sample analysis.

On the other side, Bihani et al., synthesized CNDs using lemon juice and glutathione, in which glutathione was exploited as a scaffold for the formation of carbon nanostructures [55]. The preparation of CNDs underwent the complex multistep reactions of rearrangements and cyclization reactions accompanied with a dehydration process. Indeed, the applicability prepared CNDs is limited by the constraints of uneven size distribution and agglomeration with their adjacent particles. Moreover, the synthesis of CNDs with unique surface properties and aqueous stability were not reported, limiting their prospective applications. In specific, the influences of prepared CNDs toward protein aggregation studied in this report significantly deviated the main objective of fluorescence TA sensors and the underlying molecular mechanism of CNDs for their activity was not explored. Thota et al., reported the synthesis of fluorescent CNDs from lemon grass and exploited the carbon nanostructures for living cell imaging [56]. Generally, CNDs possess the uniform quasi-spherical nanoparticles with an average diameter of < 10 nm, which is responsible for efficient fluorescence behavior, owing to the quantum confinement effect and surface defects. The obtained TEM images reveal that the carbon nanostructures demonstrate the non-uniformed spherical shape with an average size of ~ >500 nm, which not only limits their

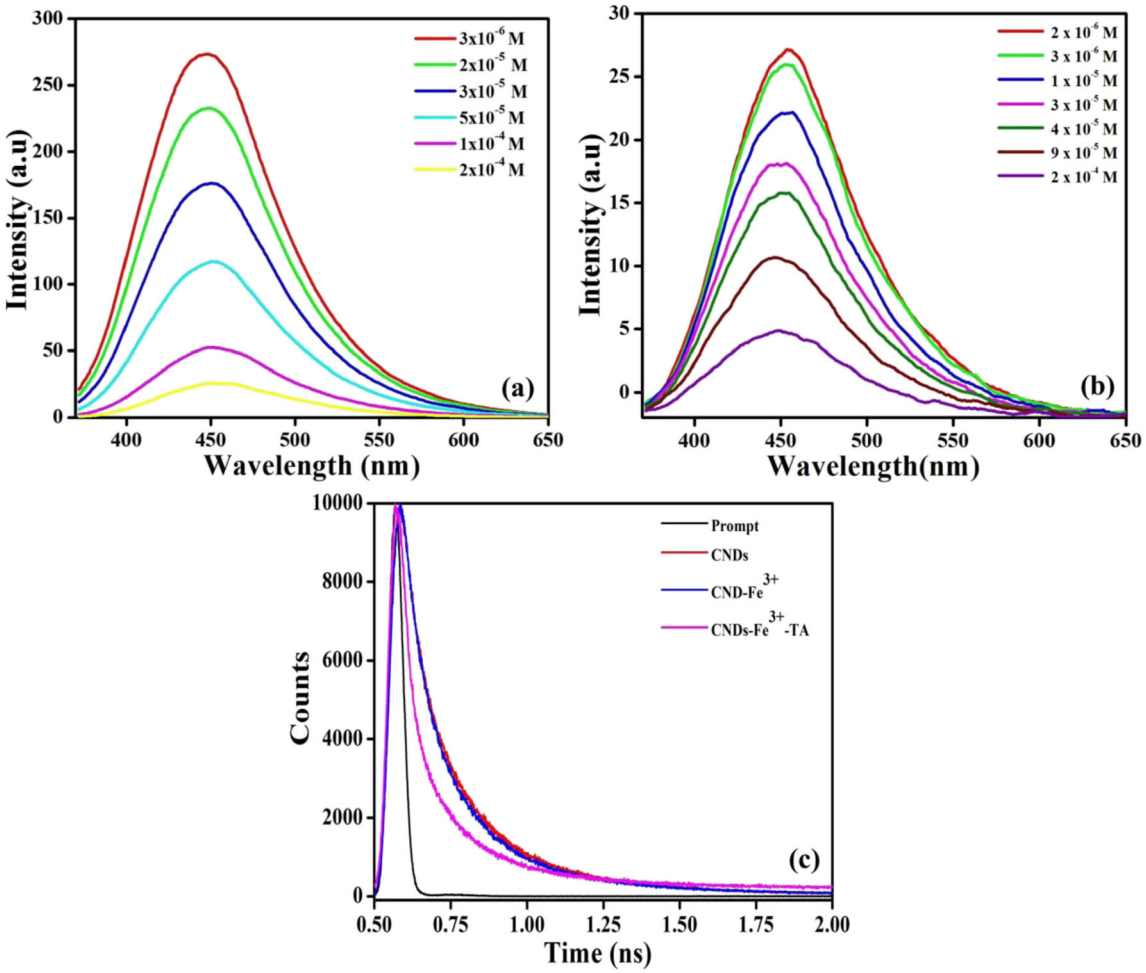

Fig. 9 Fluorescence emission of CNDs at the different concentrations of **(a)** Fe^{3+} ions and **(b)** TA spiked in river water samples, and **(c)** fluorescence decay curves of processed structures with respective of time (λ_{ex}=350 nm;λ_{em}=445 nm)

florescence behaviour but also the chemiluminescence based sensor applications. Wang et al., synthesized CNDs from different biomaterials including milk, soy-bean milk, magnolia, and silk using microwave technique [42]. However, the restraints associated with the microwave technique including utilization of sophisticated instrument, low production yield, limited applicability for polar molecules, the reflection of energy that falls on the conductive materials, and health hazards of microwave limited the utilization of above prepared CNDs. The sensing ability of CNDs towards Fe^{3+} ions was only analyzed for the optics-related applications and the detailed mechanistic pathways for the detection of Fe^{3+} ions were also not elucidated. Hence, it is clear that an immense development on CNDs is still required to explore the fluorescence based sensor applications. On the basis of these perspectives, we succeeded in the synthesis of homogeneous, highly fluorescent, hydrophilic, and bioactive CNDs via a simple hydrothermal treatment of lemon juice without any surface passive agent. The systematic methodology adopted in exploring the influences of reaction time, ionic strength, pH, excitation wavelength, and concentration of analyte provides a concrete idea on the stability of prepared CNDs. Furthermore, the detailed investigation visualized on competitive and lifetime measurement studies fundamentally intrigued the realization of prepared CNDs in real sample analysis and guaranteed its potential applications under various conditions. The influential TA fluorescence sensing properties including the lower detection limit, a wide linear range, and real sample analysis achieved for the prepared CNDs are comparable to the previous reports, which validate its prospective applications in fluorescence TA sensors.

Conclusion

In summary, CNDs were developed with a natural and inexpensive lemon extract as a sole carbon source without the aid of any passivation reagents. The prepared CNDs exhibited the excellent photoluminescent properties, remarkable water solubility, and exceptional stability. The prepared CNDs were exploited as efficient fluorescence probes for the quantification of TA under an aqueous medium, which exhibited an

excellent selectivity. The dual sensing approach of CNDs toward Fe^{3+} ions and the further utilization of CNDs-Fe^{3+} assembly toward TA detection exemplified that the consecutive sensing strategy could be beneficial for the monitoring of metal ions and biomolecules associated with the human health system. The results obtained in this report demonstrated the excellent applicability of CNDs in TA sensing, which effectively extends new channels in the advancement of high performance metal ion and biomolecule sensors.

Acknowledgements This work was supported by University Grants Commission (UGC), New Delhi, India Major Project Grant No. MRP-MAJORCHEM- 2013-36681. This work was supported by grants from the Medical Research Center Program (NRF-2017R1A5A2015061) through the National Research Foundation (NRF), which is funded by the Korean government (MSIP). This work was supported by the Korea Institute of Energy Technology Evaluation and Planning (KETEP) and the Ministry of Trade, Industry & Energy (MOTIE) of the Republic of Korea (No. 20184030202210).

Compliance with Ethical Standards

Conflict of Interest The authors declare that there are no conflicts of interest.

References

1. Kwon W, Do S, Kim JH, Jeong MS, Rhee SW (2015) Control of photoluminescence of carbon nanodots *via* surface functionalization using parasubstituted anilines. Sci Rep 5:12604 (1-10)
2. Loo AH, Sofer Z, Bousa D, Ulbrich P, Bonanni A, Pumera M (2016) Carboxylic carbon quantum dots as a fluorescent sensing platform for DNA detection. ACS Appl Mater Interface 81:951–1957
3. Cayuela A, Soriano ML, C-Carrion C, Valcarcel M (2016) Semiconductor and carbon-based fluorescent nanodots: the need for consistency. Chem Commun 52:1311–1326
4. Khan S, Verma NC, Gupta A, Nandi CK (2015) Reversible photoswitching of carbon dots. Sci Rep 5:11423 (1-7)
5. Zhai X, Zhang P, Liu C, Bai T, Li W, Dai L, Liu W (2012) Highly luminescent carbon nanodots by microwave-assisted pyrolysis. Chem Commun 48:7955–7957
6. Hsu PC, Chang HT (2012) Synthesis of high-quality carbon nanodots from hydrophilic compounds: role of functional groups. Chem Commun 48:3984–3986
7. Liu J, Liu X, Luo H, Gao Y (2014) One-step preparation of nitrogen-doped and surface-passivated carbon quantum dots with high quantum yield and excellent optical properties. RSC Adv 4: 7648–7654
8. Li Y, Zhang X, Zheng M, Liu S, Xie Z (2016) Dopamine carbon nanodots as effective photothermal agents for cancer therapy. RSC Adv 6:54087–54091
9. Long VUD, Ertek B, Dilgin Y, Cervenka L (2015) Voltammetric determination of tannic acid in beverages using pencil graphite electrode. Czech J Food Sci 33:72–76
10. Wan H, Zou Q, Yan R, Zhao F, Zeng B (2007) Electrochemistry and voltammetric determination of tannic acid on a single-wall carbon nanotube-coated glassy carbon electrode. Microchim Acta 159: 109–115
11. Chen SC, Chung KT (2000) Mutagenicity and antimutagenicity studies of tannic acid and its related compounds. Food Chem Toxicol 1:1–5
12. Ghouas H, Haddou B, Kameche M, Canselier JP, Gourdon C (2016) Removal of tannic acid from aqueous solution by cloud point extraction and investigation of surfactant regeneration by microemulsion extraction. J Surfact Deterg 19:57–66
13. Sreeram KJ, Ramasami T (2003) Sustaining tanning process through conservation, recovery and better utilization of chromium. Resour Conser Recy 38:185–212
14. Yılmaz UT, Çalık E, Uzun D, Karipcin F, Yılmaz H (2016) Selective and sensitive determination of tannic acid using a 1-benzoyl-3-(pyrrolidine) thiourea film modified glassy carbon electrode. J Electroanal Chem 776:1–8
15. Chen Z, Zhang X, Cao H, Huang Y (2013) Chitosan-capped silver nanoparticles as a highly selective colorimetric probe for visual detection of aromatic ortho-trihydroxy phenols. Analyst 138: 2343–2349
16. Zhu J, Ng J, Filippich LJ (1992) Determination of tannic acid and its phenolic metabolites in biological fluids by high-performance liquid chromatography. J Chromatogr B Biomed Sci Appl 577:77–85
17. Sun YG, Cui H, Li YH, Zhao HZ, Lin XQ (2000) Flow injection analysis of tannic acid with inhibited electrochemiluminescent detection. Anal Lett 33:2281–2291
18. Dhenadhayalan N, Lin KC (2015) Chemically induced fluorescence switching of carbon-dots and its multiple logic gate implementation. Sci Rep 5:10012 (1-10)
19. Ahmed GHG, Lainoo RB, Calzon JAG, Garcia MED (2015) Fluorescent carbon nanodots for sensitive and selective detection of tannic acid in wines. Talanta 132:252–257
20. Wang YQ, Ye C, Zhu ZH, Hu YZ (2008) Cadmium telluride quantum dots as pH-sensitive probes for tiopronin determination. Anal Chim Acta 610:50–56
21. Sahu S, Behera B, Maiti TK, Mohapatra S (2012) Simple one-step synthesis of highly luminescent carbon dots from orange juice: application as excellent bio-imaging agents. Chem Commun 48: 8835–8837
22. Lu W, Qin X, Liu S, Chang G, Chang Y, Luo Y, Asiri AM, Al-Youbi AO, Sun X (2012) Economical green synthesis of fluorescent carbon nanoparticles and their use as probes for sensitive and selective detection of mercury (II) ions. Anal Chem 84:5351–5357
23. Chang YP, Ren CL, Qu JC, Chen XG (2012) Preparation and characterization of Fe_3O_4/graphene nanocomposite and investigation of its adsorption performance for aniline and p-chloroaniline. Appl Surf Sci 261:504–509
24. Xiao L, Schroeder M, Kluge S, Balducci A, Hagemann U, Schulz C, Wiggers H (2015) Direct self-assembly of Fe_2O_3/reduced graphene oxide nanocomposite for high-performance lithium-ion batteries. J Mater Chem A 3:11566–11574
25. Zou Y, Yan F, Dai L, Luo Y, Fu Y, Yang N, Wun J, Chen L (2014) High photoluminescent carbon nanodots and quercetin-Al3+ construct a ratiometric fluorescent sensing system. Carbon 77:1148–1156
26. Zheng H, Wang Q, Long Y, Zhang H, Huang X, Zhu R (2011) Enhancing the luminescence of carbon dots with a reduction pathway. Chem Commun 47:10650–10652
27. Abbasi V, Monfared HH, Hosseini SM (2017) Mn(III)-salan/graphene oxide/magnetite nanocomposite as a highly selective catalyst for aerobic epoxidation of olefins. Appl Organomet Chem 31: 3554–3564
28. Zubir NA, Yacou C, Motuzas J, Zhang X, Da Costa JCD (2014) Structural and functional investigation of graphene oxide-Fe_3O_4 nanocomposites for the heterogeneous Fenton-like reaction. Sci Rep 4:4594

29. Xu Y, Niu X, Zhang H, Xu L, Zhao S, Chen H, Chen X (2015) Switch-on fluorescence sensing of glutathione in food samples based on a graphitic carbon nitride quantum dot (g-CNQD)-Hg^{2+} chemosensor. J Agric Food Chem 63:1747–1755
30. Ananthanarayanan A, Wang X, Routh P, Sana B, Lim S, Kim DH, Lim KH, Li J, Chen P (2014) Facile synthesis of graphene quantum dots from 3D graphene and their application for Fe^{3+} sensing. Adv Funct Mater 24:3021–3026
31. Lai T, Zheng E, Chen L, Wang X, Kong L, You C, Ruan Y, Weng X (2013) Hybrid carbon source for producing nitrogen-doped polymer nanodots: one-pot hydrothermal synthesis, fluorescence enhancement and highly selective detection of Fe(III). Nanoscale 5: 8015–8080
32. Annie Ho JA, Chang HC, Su WT (2012) DOPA-mediated reduction allows the facile synthesis of fluorescent gold nanoclusters for use as sensing probes for ferric ions. Anal Chem 84:3246–3253
33. Yang CX, Ren HB, Yan XP (2013) Fluorescent metal–organic framework MIL-53 (Al) for highly selective and sensitive detection of Fe^{3+} in aqueous solution. Anal Chem 85:7441–7446
34. Xu H, Zhou S, Xiao L, Wang H, Li S, Yuan Q (2015) Fabrication of a nitrogen-doped graphene quantum dot from MOF-derived porous carbon and its application for highly selective fluorescence detection of Fe^{3+}. J Mater Chem C 3:291–297
35. Aslandaş AM, Balcı N, Arık M, Şakiroğlu H, Onganer Y, Meral K (2015) Liquid nitrogen-assisted synthesis of fluorescent carbon dots from blueberry and their performance in Fe^{3+} detection. Appl Surf Sci 356:747–752
36. Sachdev A, Gopinath P (2015) Green synthesis of multifunctional carbon dots from coriander leaves and their potential application as antioxidants, sensors and bioimaging agents. Analyst 140:4260–4269
37. Nguyen V, Yan L, Si J, Hou X (2016) Femtosecond laser-assisted synthesis of highly photoluminescent carbon nanodots for Fe^{3+} detection with high sensitivity and selectivity. Opt Mater Express 6: 312–320
38. Qu K, Wang J, Ren J, Qu X (2013) Carbon dots prepared by hydrothermal treatment of dopamine as an effective fluorescent sensing platform for the label-free detection of iron (III) ions and dopamine. Chem Eur J 19:7243–7249
39. Yu J, Xu C, Tian Z, Lin Y, Shi Z (2016) Facilely synthesized N-doped carbon quantum dots with high fluorescent yield for sensing Fe^{3+}. New J Chem 40:2083–2088
40. Murugan N, Sundramoorthy AK (2018) Green synthesis of fluorescent carbon dots from Borassusflabellifer flowers for label-free highly selective and sensitive detection of Fe^{3+} ions. New J Chem 42:13297–13307
41. Chen Z, Lu D, Zhang G, Yang J, Dong C, Shuang S (2014) Glutathione capped silver nanoclusters-based fluorescent probe for highly sensitive detection of Fe^{3+}. Sens Actuator B-Chem 202:631–637
42. Wang J, Peng F, Lu Y, Zhong Y, Wang S, Xu M, Ji X, Su Y, Liao L, He Y (2015) Large-scale green synthesis of fluorescent carbon nanodots and their use in optics applications. Adv Opt Mater 3: 103–111
43. Liu W, Diao H, Chang H, Wang H, Li T, Wei W (2017) Green synthesis of carbon dots from rose-heart radish and application for Fe^{3+} detection and cell imaging. Sensors Actuators B Chem 241: 190–198
44. Zhang H, Chen Y, Liang M, Xu L, Qi S, Chen H, Chen X (2014) Solid-phase synthesis of highly fluorescent nitrogen-doped carbon dots for sensitive and selective probing ferric ions in living cells. Anal Chem 86:9846–9852
45. Hamishehkar H, Ghasemzadeh B, Naseri A, Salehi R, Rasoulzadeh F (2015) Carbon dots preparation as a fluorescent sensing platform for highly efficient detection of Fe (III) ions in biological systems. Spectrochim Acta A Mol Biomol Spect 150:934–939
46. Liu W, Diao H, Chang H, Wang H, Li T, Wei W (2017) Green synthesis of carbon dots from rose-heart radish and application for Fe^{3+} detection and cell image. Sens Actuators B Chem 241:190–198
47. Huang CP, Dong C, Tang Z (1993) Advanced chemical oxidation: its present role and potential future in hazardous waste treatment. Waste Manag 13:361–377
48. Zhang S, Li J, Zeng M, Xu J, Wang X, Hu W (2014) Polymer nanodots of graphitic carbon nitride as effective fluorescent probes for the detection of Fe^{3+} and Cu^{2+} ions. Nanoscale 6:4157–4162
49. Dhenadhayalan N, Lin KC, Suresh R, Ramamurthy P (2016) Unravelling the multiple emissive states in citric-acid-derived carbon dots. J Phy Chem C 120:1252–1261
50. Chen RL, Lin CH, Chung CY, Cheng TJ (2005) Determination of tannin in green tea infusion by flow-injection analysis based on quenching the fluorescence of 3-aminophthalate. J Agr Food Chem 53:8443–8446
51. Xu L, He N, Du J, Deng Y, Li Z, Wang T (2009) A detailed investigation for determination of tannic acid by anodic stripping voltammetry using porous electrochemical sensor. Anal Chim Acta 634:49–53
52. Liu Y, Han S (2017) Chemiluminescence of nitrogen-doped carbon quantum dots for the determination of Thiourea and tannic acid. Food Anal Methods 10:3398–3406
53. Sinduja B, John SA (2016) Sensitive determination of tannic acid using blue luminescent graphene quantum dots as fluorophore. RSC Adv 6:59900–59906
54. De B, Karak N (2013) A green and facile approach for the synthesis of water soluble fluorescent carbon dots from banana juice. RSC Adv 3:8286–8290
55. Bihani O, Rai T, Panda D (2018) Interaction of proteins with lemon-juice/glutathione-derived carbon nanodot: interplay of induced-aggregation and cosolubilization. Int J Biol Macromol 112:1234–1240
56. Thota SP, Thota SM, Bhagavatham SS, Manoj KS, Muthukumar VSS, Venketesh S, Vadlani PV, Belliraj SK (2017) Facile one-pot hydrothermal synthesis of stable and biocompatible fluorescent carbon dots from lemon grass herb. IET Nanobiotechnol 12:127–132